Electronic Supplementary Material (ESI) for Journal of Materials Chemistry A.

Supporting Information

High-Efficiency Ultrathin Flexible Organic Solar Cells with a Bilayer Hole Transport Layer

Dongyang Zhang[1], Yitong Ji[1], Yingying Cheng[1], Xiangda Liu[1], Zezhou Xia[1], Xiujun Liu[1], Xiaotong Liu[1], Xueyuan Yang[1], Wenchao Huang[1]*

Key state Laboratory of Advanced Technology for Materials Synthesis and Processing, School of Materials Science and Engineering, Wuhan University of Technology, 430070, Wuhan, China

Corresponding E-mail: wenchao.huang@whut.edu.cn

Experimental details

Materials: PM6, L8-BO, and PDINN were purchased from Solarmer Materials Inc, Beijing. Poly(3,4-ethylene dioxythiophene): poly(styrenesulfonate) (PEDOT:PSS) aqueous solution (Clevios PVP 4083) was purchased from Heraeus, Germany. All other chemicals were purchased from Aladdin and used without further purification.

Ultrathin Device Fabrication: The ultrathin OSCs were fabricated with a structure of parylene/ITO/MoO_3/PEDOT:PSS/PM6:L8-BO/PDINN/Ag. First, the fluorinated polymer layer (Novec 1700:7100) was spin-coated on the pre-cleaned glass substrates at 4000 rpm for 1 min. Then, ultrathin parylene film was subsequently deposited on the fluoropolymer-coated glass substrates using chemical vapor deposition. A 180 nm indium tin oxide (ITO) film was sputtered and patterned using a mask, with a sheet resistance of 28 Ohm/sq. Then, MoO_3 was thermally deposited at a vacuum pressure of $\sim 1\times10^{-4}$ Pa. Next, PEDOT:PSS was spin-coated at 5000 rpm for 40 s and annealed on a hot stage in the air at 150 °C for 15 min. The PM6:L8-BO solution (1:1.2 by weight and total concentration of 16 mg/mL in chloroform with 0.5% 1,8-diiodooctane (DIO, v/v) additive) was stirred at 45 °C for 2 h before spin-coated at a speed of 4000 rpm for 30 s. The active layer thickness is around 110 nm. The active layers were annealed at 100 °C for 5 min. Subsequently, PDINN in methanol solutions (0.8 mg/mL) was spin-coated on the active layers at 3000 rpm for 40 s. Finally, Ag (110 nm) was thermally deposited as an electrode at a vacuum pressure of $\sim 1\times10^{-4}$ Pa.

Characterizations:

The absorption and transmission spectra were measured with an ultraviolet spectrometer (Shimadzu UV–1900i). Film thickness was measured by a Dektak XT probe profiler (produced by Bruker). Photovoltaic parameters and mechanical stability of ultrathin devices are tested in a nitrogen glove box. The *J-V* curve of the device was tested using a Keithley 2450 source measure unit under standard sunlight provided by a sunlight simulator (SS-X50, Enlitech). A metal mask with an area of 0.04 cm^2 was used to define the effective area of the devices. The measurements were conducted using a voltage scan range of -0.2 to 1.0 V. All photovoltaic parameters of devices are averaged over 20 devices. Mechanical stability of ultrathin OSCs is tested using an automated tensile-bending tester (PR-BDM4-100V). Mechanical stability of ultrathin OSCs is averaged over 8 devices. The light intensity was calibrated using a standard silicon reference cell certified by the National Renewable Energy Laboratory (NREL, USA). The EQE was obtained using a solar cell spectral response measurement system (Enli Technology Co., Ltd., QE-R). The light intensity of the system is calibrated by the reference Si probe (RC-S103011-E) obtained from Enli Technology Co Ltd. TPC and TPV were measured using a transient photocurrent and photovoltage measurement system (LST-TPC, Shanghai Jinzhu Technology Co., Ltd.). The morphology of the films is characterized by atomic force microscope (AFM). Grazing-incidence wide-angle X-ray scattering (GIWAXS) patterns were measured using Xeuss 3.0 system. The 10 keV X-ray beam was incident at a grazing angle of 0.15°.

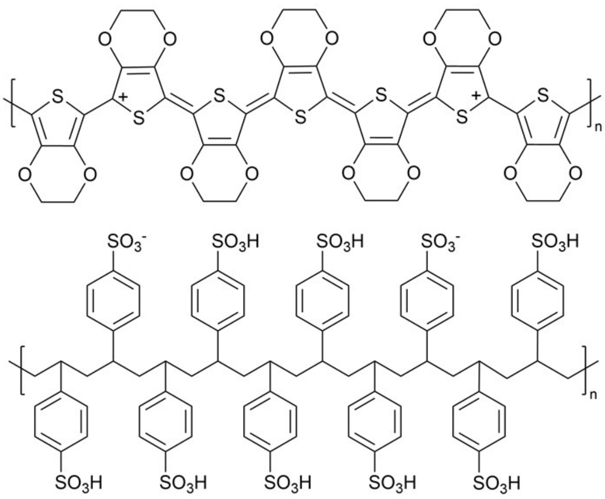

Figure S1. Chemical structure of PEDOT:PSS.

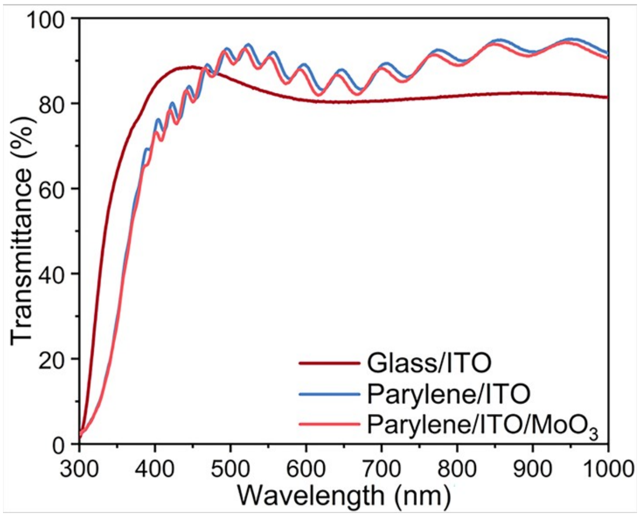

Figure S2. Transmittance spectra of glass/ITO, parylene/ITO and parylene/ITO/MoO_3.

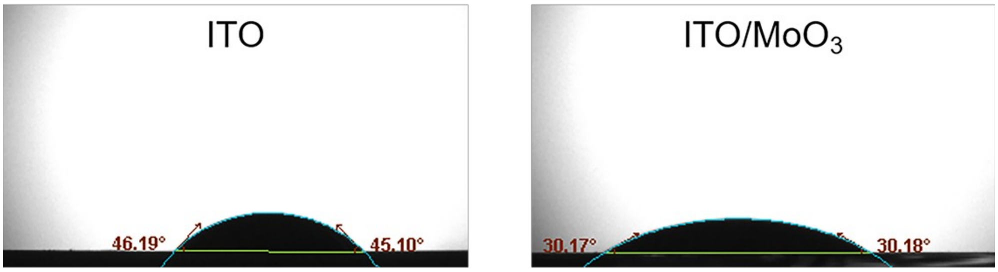

Figure S3. Contact angles for PEDOT:PSS on parylene/ITO and parylene/ITO/MoO_3 samples.

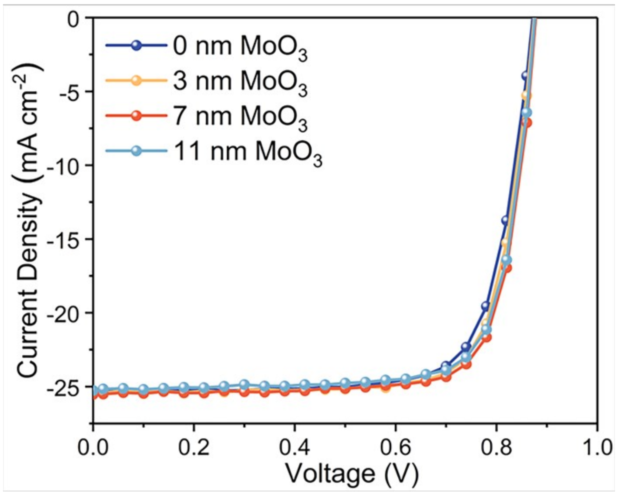

Figure S4. *J-V* curves of PM6:L8-BO-based ultrathin OSCs with different MoO_3 thickness.

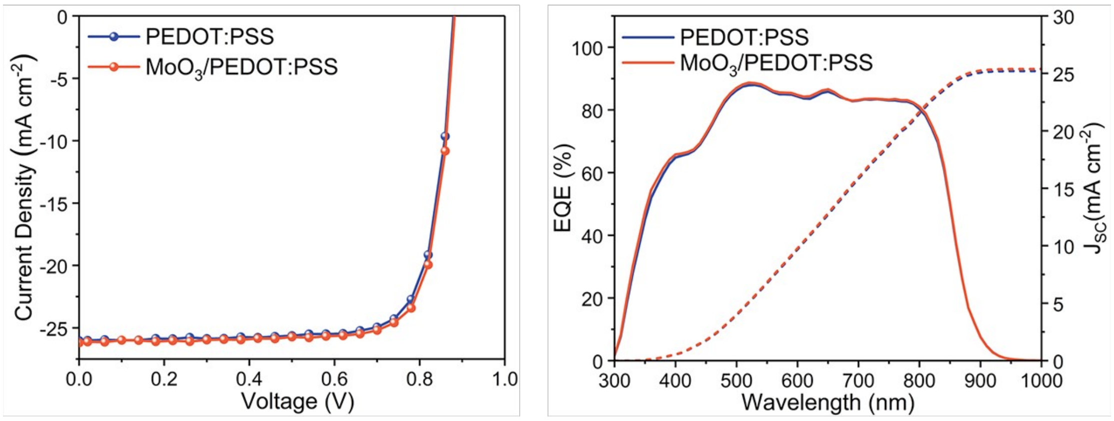

Figure S5. *J-V* curves and EQE spectra of rigid PM6:L8-BO OSCs.

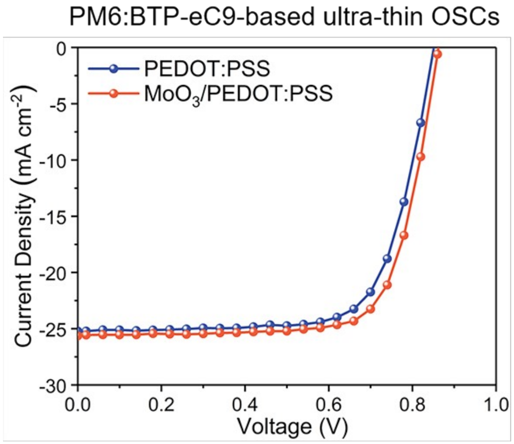

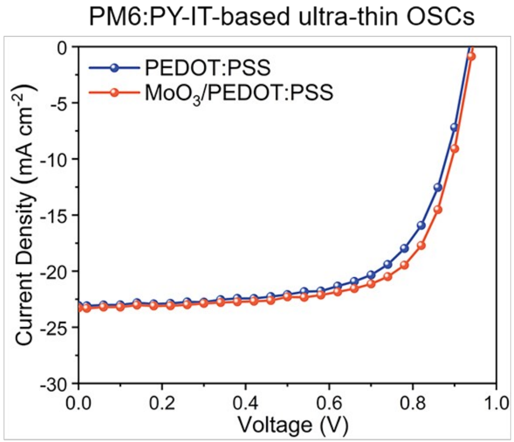

Figure S6. *J-V* curves of PM6:BTP-eC9-based and PM6:PY-IT-based ultrathin OSCs.

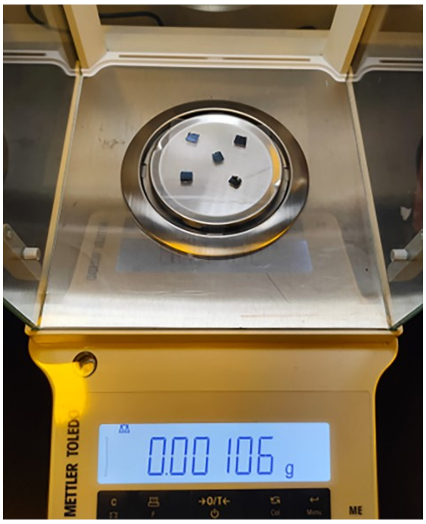

Figure S7. The weight of five 0.7 cm * 0.7 cm ultrathin OSCs.

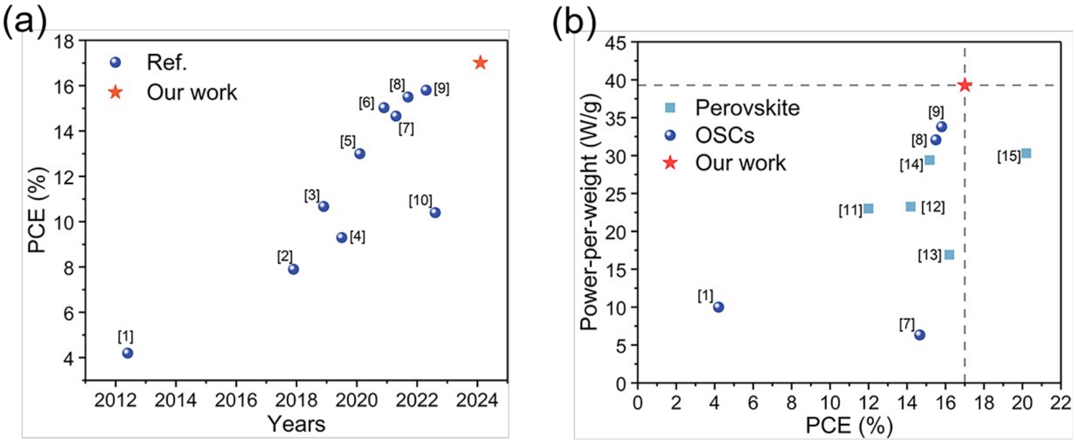

Figure S8. Summary of PCE and power-per-weight of bottom-illuminated ultrathin OSCs reported in previous literatures.

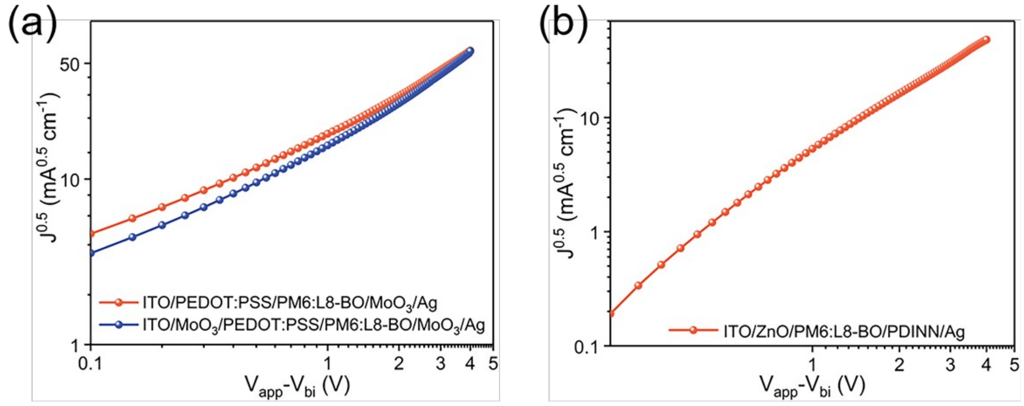

Figure S9. $J^{0.5}$-V curves of the (a) hole-only and (b) electron-only devices.

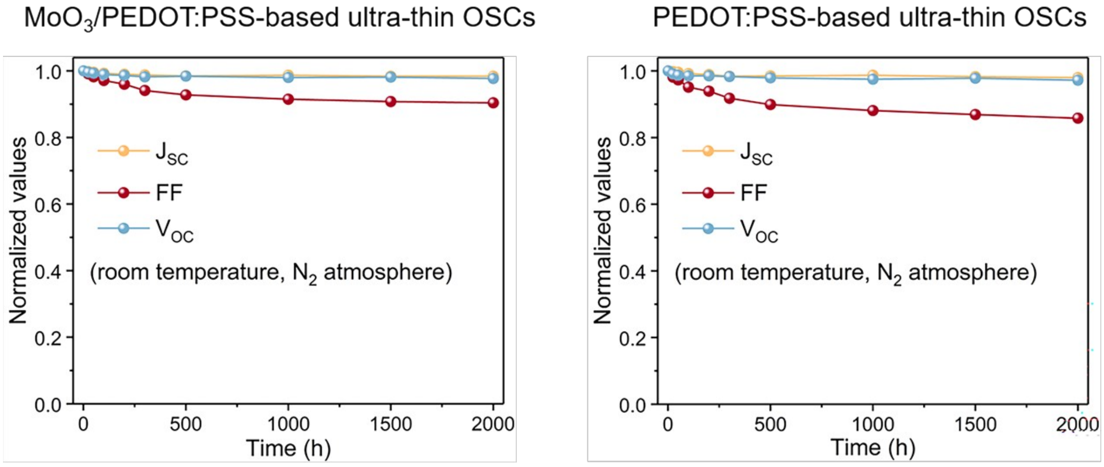

Figure S10. Evolution of V_{OC}, J_{SC} and FF of ultrathin OSCs stored in N_2 at 25 °C under dark conditions: (a) MoO_3/PEDOT:PSS-based OSCs and (b) PEDOT:PSS-based OSCs.

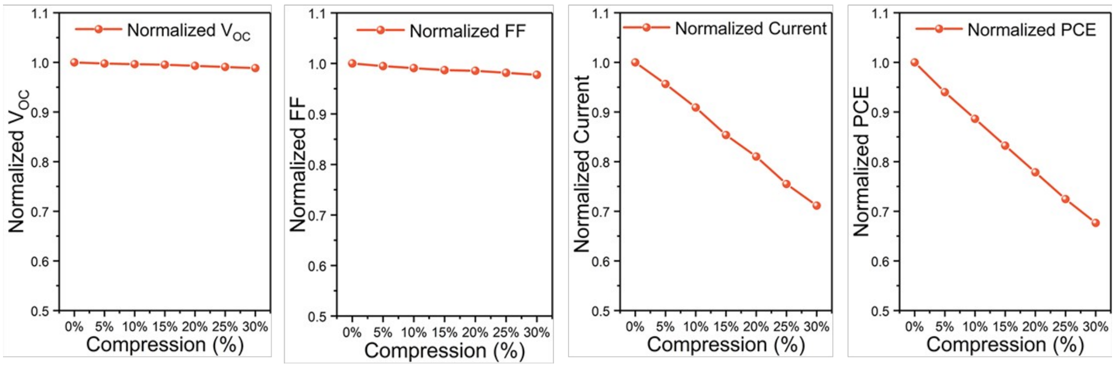

Figure S11. Trends of photovoltaic parameters of ultrathin OSCs at different compression rates.

Table S1. Photovoltaic parameters of PM6:L8-BO-based ultrathin OSCs with different MoO_3 thickness.

	V_{OC} [V]	J_{SC} [mA cm^{-2}]	FF [%]	PCE [%]
0 nm MoO_3	0.879 (0.866±0.004)	25.3 (25.1±0.2)	74.4 (74.0±0.4)	16.4 (16.1±0.3)
3 nm MoO_3	0.872 (0.868±0.004)	25.4 (25.2±0.3)	75.6 (75.1±0.5)	16.7 (16.4±0.3)
7 nm MoO_3	0.873 (0.871±0.002)	25.5 (25.3±0.3)	76.4 (76.1±0.4)	17.0 (16.7±0.3)
11 nm MoO_3	0.873 (0.871±0.002)	25.1 (24.9±0.3)	76.2 (76.1±0.3)	16.7 (16.5±0.2)

Table S2. Photovoltaic parameters of PM6:L8-BO-based rigid OSCs with and without MoO_3 interlayer.

HTL	V_{OC} [V]	J_{SC} [mA cm^{-2}]	J_{cal} [mA cm^{-2}]	FF [%]	PCE [%]
PEDOT:PSS	0.872 (0.871±0.003)	26.0 (25.9±0.2)	25.2	78.1 (77.6±0.5)	17.7 (17.5±0.2)
MoO_3/PEDOT:PSS	0.879 (0.877±0.002)	26.2 (26.0±0.2)	25.4	78.6 (78.3±0.4)	18.1 (17.8±0.3)

Table S3. Photovoltaic parameters of PM6:BTP-eC9-based and PM6:PY-IT-based ultrathin OSCs.

Active layer	HTL	V_{OC} [V]	J_{SC} [mA cm^{-2}]	FF [%]	PCE [%]
PM6:BTP-eC9	PEDOT:PSS	0.848 (0.847±0.002)	25.2 (24.9±0.3)	70.9 (70.6±0.4)	15.2 (15.1±0.1)
	MoO_3/PEDOT:PSS	0.859 (0.859±0.003)	25.6 (25.4±0.2)	72.7 (72.3±0.5)	16.0 (15.8±0.2)
PM6:PY-IT	PEDOT:PSS	0.932 (0.931±0.002)	23.2 (22.9±0.3)	66.3 (66.1±0.4)	14.3 (14.1±0.2)
	MoO_3/PEDOT:PSS	0.940 (0.938±0.002)	23.3 (23.0±0.3)	68.8 (68.5±0.3)	15.1 (15.0±0.1)

Table S4. R_{series} and R_{shunt} of ultrathin OSCs with and without MoO_3 interlayer.

HTL	R_{series} [Ωcm^2]	R_{shunt} [Ωcm^2]
PEDOT:PSS	1.07	1.15×10^7
MoO_3/PEDOT:PSS	1.13	4.20×10^7

Table S5. Photovoltaic parameters of the best-performing ultrathin OSCs with a large area of 0.49 cm^2.

HTL	V_{OC} [V]	J_{SC} [mA cm^{-2}]	FF [%]	PCE [%]
PEDOT:PSS	0.862 (0.861±0.002)	25.1 (25.0±0.2)	70.9 (70.6±0.4)	15.3 (15.1±0.3)
MoO_3/PEDOT:PSS	0.872 (0.869±0.003)	25.3 (25.1±0.2)	74.8 (74.4±0.4)	16.5 (16.3±0.2)

Table S6. Photovoltaic parameters of stretchable OSCs with device area of 0.04 cm^2 at different compression rates.

Compression (%)	V_{OC} [V]	Current [mA]	FF [%]	PCE [%]
0	0.873 (0.871±0.002)	1.02 (1.01±0.01)	76.0 (75.7±0.4)	16.9 (16.7±0.2)
5	0.871 (0.869±0.002)	0.97 (0.97±0.01)	75.5 (75.3±0.3)	15.9 (15.7±0.2)
10	0.870 (0.868±0.003)	0.92 (0.92±0.01)	75.2 (75.0±0.3)	15.0 (14.8±0.3)
15	0.869 (0.867±0.002)	0.87 (0.86±0.01)	74.8 (74.7±0.3)	14.1 (13.9±0.2)
20	0.867 (0.865±0.003)	0.82 (0.82±0.01)	74.7 (74.6±0.2)	13.3 (13.0±0.3)
25	0.864 (0.863±0.003)	0.77 (0.76±0.01)	74.5 (74.3±0.3)	12.4 (12.1±0.3)
30	0.862 (0.861±0.003)	0.72 (0.72±0.01)	74.3 (74.0±0.3)	11.5 (11.3±0.3)

Table S7. The statistical data for bottom-illuminated ultrathin solar cells.

Type	Device structure	PCE [%]	Power-per-weight [W/g]	Years	Ref.
OSC	PET/PEDOT:PSS/P3HT:PCBM/Ca/Ag	4.2	10	2012.4	1
	Parylene/ITO/ZnO/PNTz4T:$PC_{71}BM$/MoO3/Ag	7.9	-	2017.9	2
	Parylene/ITO/ZnO/PBDTTT-OFT:$PC_{71}BM/MoO_3$/Ag	10.67	-	2018.9	3
	PI/ITO/ZnO/PTzNTz-BOBO:$PC_{71}BM/MoO_3$/Ag	9.3	-	2019.5	4
	Parylene/SU8/ITO/ZnO/PBDTTT-OFT:IEICO-4F:$PC_{71}BM/MoO_3$/Ag	13.0	-	2020.1	5
	PEN/AgNWs/PEI-Zn/PM6:Y6/MoO_3/Ag	15.03	-	2020.9	6
	PE/PH1000/Al4083/PM6:Y6/PFN-Br/Al	14.66	6.33	2021.3	7
	PET/PH1000/PEDOT:PSS(4083)/ D18-Cl:Y6:$PC_{71}BM$/PFNDI-Br/Ag	15.5	32.07	2021.7	8
	tPI/ITO/PEI-Zn/PM6:Y6/MoO_3/Ag	15.8	33.80	2022.3	9
	Parylene/ITO/ZnO/PBDTTT-OFT: IEICO-4F/PEDOT:PSS/Ag	10.4	-	2022.6	10
	Parylene/ITO/MoO_3/PEDOT:PSS/ PM6:L8-BO/PDINN/Ag	17.01	39.3	Our work	
PSC	PET/PEDOT:PSS/Perovskite/PTCDI Cr_2O_3/Au	12.0	23.0	2015.9	11
	PET/ITO/NiOx/Perovskite/C60/Bis-C60/Ag	14.19	23.26	2017.4	12
	PET/ITO/NiOx/R-BA /Perovskite/PCBM/Bis-C60/Ag	16.2	16.9	2017.9	13
	PEN/AgNWs/PH1000/Al4083/ Perovskite/$PC_{61}BM$/Al	15.18	29.4	2019.1	14
	Parylene/ITGZO/PTAA/Perovskite /PCBM/BCP/Cu	20.2	30.3	2022.9	15

Reference

1 M. Kaltenbrunner, M. S. White, E. D. Głowacki, T. Sekitani, T. Someya, N. S. Sariciftci and S. Bauer, *Nat. Commun.*, 2012, **3**, 770.

2 H. Jinno, K. Fukuda, X. Xu, S. Park, Y. Suzuki, M. Koizumi, T. Yokota, I. Osaka, K. Takimiya and T. Someya, *Nat. Energy*, 2017, **2**, 780–785.

3 S. Park, S. W. Heo, W. Lee, D. Inoue, Z. Jiang, K. Yu, H. Jinno, D. Hashizume, M. Sekino, T. Yokota, K. Fukuda, K. Tajima and T. Someya, *Nature*, 2018, **561**, 516–521.

4 H. Kimura, K. Fukuda, H. Jinno, S. Park, M. Saito, I. Osaka, K. Takimiya, S. Umezu and T. Someya, *Adv. Mater.*, 2019, **31**, 1808033.

5 W. Huang, Z. Jiang, K. Fukuda, X. Jiao, C. R. McNeill, T. Yokota and T. Someya, *Joule*, 2020, **4**, 128–141.

6 F. Qin, W. Wang, L. Sun, X. Jiang, L. Hu, S. Xiong, T. Liu, X. Dong, J. Li, Y. Jiang, J. Hou, K. Fukuda, T. Someya and Y. Zhou, *Nat. Commun.*, 2020, **11**, 4508.

7 J. Wan, R. Wen, Y. Xia, M. Dai, H. Huang, L. Xue, Z. Zhang, J. Fang, K. N. Hui and X. Fan, *J. Mater. Chem. A*, 2021, **9**, 5425–5433.

8 W. Song, K. Yu, E. Zhou, L. Xie, L. Hong, J. Ge, J. Zhang, X. Zhang, R. Peng and Z. Ge, *Adv. Funct. Mater.*, 2021, **31**, 2102694.

9 S. Xiong, K. Fukuda, S. Lee, K. Nakano, X. Dong, T. Yokota, K. Tajima, Y. Zhou and T. Someya, *Adv. Sci.*, 2022, **9**, 2105288.

10 S. I. Rich, S. Lee, K. Fukuda and T. Someya, *Adv. Mater.*, 2022, **34**, 2106683.

11 M. Kaltenbrunner, G. Adam, E. D. Głowacki, M. Drack, R. Schwödiauer, L. Leonat, D. H. Apaydin, H. Groiss, M. C. Scharber, M. S. White, N. S. Sariciftci and S. Bauer, *Nat. Mater.*, 2015, **14**, 1032–1039.

12 H. Zhang, J. Cheng, D. Li, F. Lin, J. Mao, C. Liang, A. K.-Y. Jen, M. Grätzel and W. C. H. Choy, *Adv. Mater.*, 2017, **29**, 1604695.

13 Q. Wang, C.-C. Chueh, T. Zhao, J. Cheng, M. Eslamian, W. C. H. Choy and A. K.-Y. Jen, *ChemSusChem*, 2017, **10**, 3794–3803.

14 S. Kang, J. Jeong, S. Cho, Y. J. Yoon, S. Park, S. Lim, J. Y. Kim and H. Ko, *J. Mater. Chem. A*, 2019, **7**, 1107–1114.

15 J. Wu, P. Chen, H. Xu, M. Yu, L. Li, H. Yan, Y. Huangfu, Y. Xiao, X. Yang, L. Zhao, W. Wang, Q. Gong and R. Zhu, *Sci. China Mater.*, 2022, **65**, 2319–2324.